# An Investigation in Applying Image Retrieval Techniques to X-Ray Engineering Pictures

RAOUL PASCAL PEIN
Univ. of Huddersfield
Dept. of Informatics
Queensgate
Huddersfield HD1 3DH
UNITED KINGDOM
r.p.pein@hud.ac.uk

JOAN LU
Univ. of Huddersfield
Dept. of Informatics
Queensgate
Huddersfield HD1 3DH
UNITED KINGDOM
z.lu@hud.ac.uk

JOHN BIRGER STAV
Sør-Trøndelag Univ. College
Dept. of Technology
N-7004 Trondheim
NORWAY
John.B.Stav@hist.no

MIRO URAN
Institut za Varilstvo
Ptujska 19
1000 Ljubljana
SLOVENIA
miro.uran@i-var.si

*Abstract:* Using image retrieval techniques in analysing Non-destructive testing reults is a new challenge in both computing science and engineering applications. Objective of this research is to develop an image retrieval system to analyse X-ray images for welding industry. The content based image retrieval has been used in this investigation, particularly in feature vector paradigm and similarity as well as detailed analysis towards single defects. It is found that X-ray images can be digitally analysed qualitatively and quantitatively easily. It concludes that the use of existing CBIR techniques can provide a platform to quickly develop new image analysis tools.

*Key–Words:* Content-based image retrieval, Image analysis, X-ray, Welding defect, Feature vector

## 1 Introduction

Using image retrieval techniques in analysing Non-destructive testing reults is a new challenge in both computing science and engineering applications. The techniques of Content-Based Image Retrieval (CBIR) systems can be applied in various environments. Not only obvious areas such as image libraries [1, 16] can benefit, but also other application domains. The importance of CBIR is especially increasing in medical applications, where many of X-ray images are produced for diagnosis [11, 8, 10]. Also the engineering sector investigates possible applications, such as 3D model retrieval [4, 3, 12].

It has been known that in welding industry, non destructive testing could produce a huge amount of images in the forms of photos, digital images or X-ray pictures containing different types of welding defects which are vital for the quality of industrial products. However, advanced image retrieval techniques are rarely applied into the field of welding, particularly for analyzing welding defects taken by x-ray pictures. It follows that research into developing an advanced system for retrieving, analyzing, classifying and recognizing welding defects is of interest in both academic study and industrial applications. The objective of this research is to develop an advanced image retrieval system to achieve retrieving, analyzing and classifying welding images for different types of pictures efficiently and accurately.

## 2 Methods

In this investigation, the key methods and mechanisms involved are related to CBIR. Content Based Image Retrieval is a technique which can retrieve a large collection of images based on their features, such as texture, color and shape. Especially for the X-ray pictures, which present welding defects, both techniques of color and shape identification are extremely useful. Images are normally stored in and retrieved from an image repository. The latest development in CBIR is to achieve filling a gap between micro-level's pixel graphic contents and macro-level's image meanings, i.e. semantic retrieval [9, 7, 13].

The challenge of this research is the semantic gap between the pixels and the semantics cannot be completely closed with current technology [5]. Thus, the intended software is developed in several steps with methods specific for the given application domain.

Architecture of the system is designed based on the CBIR mechanisms [15]. It is in three levels: abstract, generic and specific (Fig. 1). It is clear that the system is generic and dynamic. Digital images of welding samples can be retrieved for visualization and assessment.

The proposed system relies on two basic methodologies. For classifying and ranking several related images, the feature vector paradigm is adapted. It enables the fat comparison of two images, without the need of analyzing the images completely each time. In order to enable the computer to "understand" more of the image semantics, techniques from image recognition need to be applied, which is more effective and more complicated to achieve.

### 2.1 Feature vector paradigm and similarity

In the field of CBIR, the use of feature vectors to describe an image is very popular [6]. A major part of this investigation is rooted in this paradigm. The aim is to develop a set of feature vectors that actually describe the severity of different fault types. Depending on the characteristics of each fault type, different bits information can be extracted from the original images. These features can be very simple or very sophisticated. Based on those features, a set of kindred images can be ranked by severity of the faults.

### 2.2 Detailed analysis towards single defects

Due to the wide range of possible fault types in an image, it is necessary to develop a specific algorithm for each fault. While it is not expected to return perfectly reliable results, the automatic analysis can already give some direct feedback. This can help engineers to spot potential faults. It is assumed that even simple approaches already provide several benefits to the user. Hence, in productive environments, much additional work will be required in the end.

## 3 System design

The foundation of the analysis tool is laid by a CBIR system, capable of linking different feature vector modules into the system (Fig. 1). The core service is the *RetrievalServer*, managing the attached components. The *Ranker* is responsible to generate and sort the results for each retrieval and uses the text based *LuceneStorage* as well as the CBIR based *FeatureVectorStorages*. Each of these storage classes represents a single feature vector. In order to generate a domain specific ranking, special feature vector modules are attached here.

A set of feature vector modules is being developed and plugged into the retrieval system. Each module is capable of extracting one specific bit of information from any source image. Every module is either aimed at a generic feature vector for retrieval or a domain specific use case. Section 4 describes two different feature vectors for welding engineers.

## 4 Implementation

A previously developed CBIR system [14, 15] is used to test these new feature vectors and compare their performance. Each newly developed feature vector can be wrapped into a plug-in and registered with the engine. It is possible to use the default user interface for querying, as the query language [13] can handle the extensions easily.

### 4.1 Spotting dark areas

One feature developed - *darkarea* - can carry out a straight forward analysis of the darkest areas in the sample images. Many faults cause a different material density compared to the surrounding area. In X-ray images, defects such as cracks and inclusions are typically much darker than the surrounding area. Searching for these areas is a very straightforward attempt to measure the relative material quality. The dataset consists of two values: the percentage of dark areas and the threshold between dark and bright pixels. The *darkarea* feature converts the image into 256 tone grey scale for further processing.

The percentage $pc$ is determined by counting the amount of pixels below a fixed threshold (e.g. 50) and calculating the relation between the amount of black pixels $n_b$ and all image pixels $n_a$:

$$pc = \frac{n_b}{n_a} \tag{1}$$

The threshold between the dark and bright pixels is determined with the help of a histogram that contains bins for each brightness level $x_i$. The threshold $th$ is the smallest value, where $1\%$ of all pixels are darker:

$$th : \left( \frac{1}{n_a} * \sum_{i=0}^{th} x_i \right) > 0.01 \tag{2}$$

For the comparison of two images, the two parameters of the images (A, B) are used to calculate the similarity $s_{AB}$, which is a normalized value between 0 and 1. The difference between the parameters of each image is calculated and normalized. The normalised values are $th_{AB}$ (Equ. 3) and $pc_{AB}$ (Equ. 4).

$$th_{AB} = \frac{\|th_A - th_B\|}{256} \tag{3}$$

$$pc_{AB} = \|pc_A - pc_B\| \tag{4}$$

The overall similarity $s_{AB}$ is constructed as the weighted sum of $th_{AB}$ and $pc_{AB}$. Currently, both features are equally weighted with $\frac{1}{2}$. As the intermediate result is 0 for identity, it is subtracted from 1. In order to emphasize differences, the result is squared.

$$s_{AB} = \left(1 - \left(\frac{1}{2} th_{AB} + \frac{1}{2} pc_{AB}\right)\right)^2 \tag{5}$$

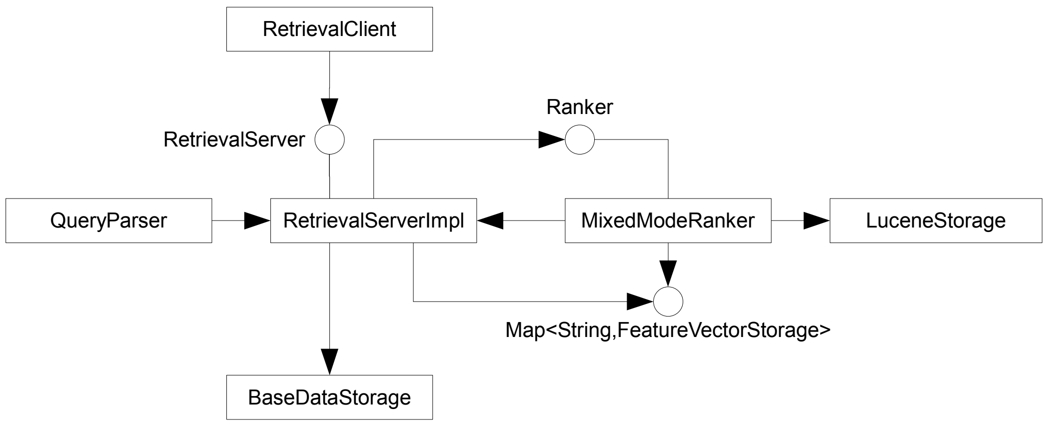


Figure 1: Core Classes

### 4.2 Finding spherical defects

The second feature - *gaspore* - is much more specialized. The algorithm tracks for round shapes in the image and attempts to fit them to circles with position and radius. For each image, a set of potential spherical defects, such as gas pores, can be determined, consisting of the circle definitions found. Dependent on this feature, the porosity of a material can be assessed.

In this investigation, a simple approach based on a Hough transformation [2] is applied. In the current algorithm it is assumed that the background is largely free of noise and relatively homogeneous. By converting the original image into a black/white representation, the areas of interest are supposed to protrude from the background, as they are expected to be much darker. The efficiency of this conversion relies on a well balanced threshold to suppress the remaining noise. The resulting pixel areas are then clustered and the Hough transformation is used to find the best match for each cluster.

The extracted set of circles is a measure for material porosity. In the current evaluation, only the amount of discovered circles is used for comparison. More detailed characteristics are to be developed later on.

## 5 Testing and Evaluation

### 5.1 Data preparation

To measure the efficiency of the feature vectors, a set of multiple x-ray images of welding seams is used. The testing set consists of several images depicting a high gaseous porosity in a long welding seam. To minimize the effect of noise and different boundary conditions of the various x-ray radiographs provided, each image is evaluated on its own. The original images are split into 8 equally sized sub image, each one showing a short segment of the seam. Due to the inhomogeneous seam porosity, each segment shows a different amount of gas pores.

### 5.2 Testing procedures

For each test, exactly one image set is used in the retrieval. The segment with the highest porosity is manually chosen and used as a query image. The CBIR system then creates a ranking dependent on the feature similaritiy described above. It is expected that the corresponding images from the same photography are then ordered by fault severity. The testing procedure for each image is as follows:

1. Splitting into 8 sub-images
2. Extraction of all feature vectors
3. Manual choice of section with highest porosity as query
4. Automatical ranking of the related images
5. Analysis of results

In most cases, the results were close to the expectations. The tests failed on some images with low contrast between defect and background, because the extraction algorithms rely on very dark areas. Other test images have a very homogeneous distribution of porosity and are therefore not suitable for an expressive analysis.

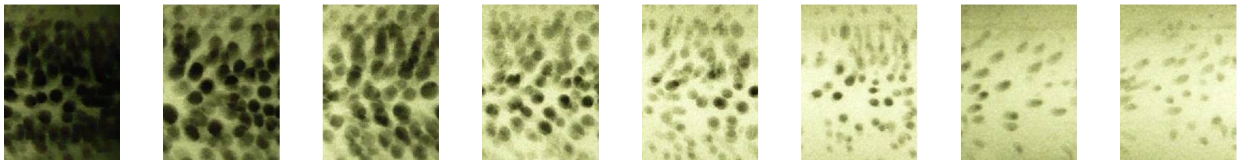

(a) (b) (c) (d) (e) (f) (g) (h)

Figure 2: Sorted Results A

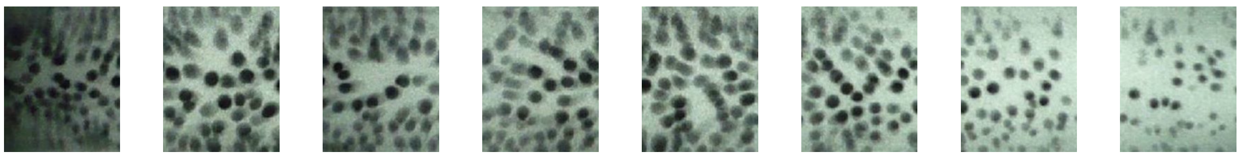

(a) (b) (c) (d) (e) (f) (g) (h)

Figure 3: Sorted Results B

# 6 Results

Two test results are presented in Figs. 2 (set A) and 3 (set B). Each set originates from an X-ray image of a single welding seam.

Test set A shows a higher variation in its defect density than set B. While image (Fig. 2(a)) contains a high amount of black areas, the last one in the series (Fig. 2(h)) is only spotted with few relatively small and lightly grey defects.

Set B is visually more homogenous. The first image (Fig. 3(c)) is very dark, but brighter than the darkest one of set A. The defects in the subsequent images show a relatively even distribution, especially the five images from Fig. 3(d) to Fig. 3(g).

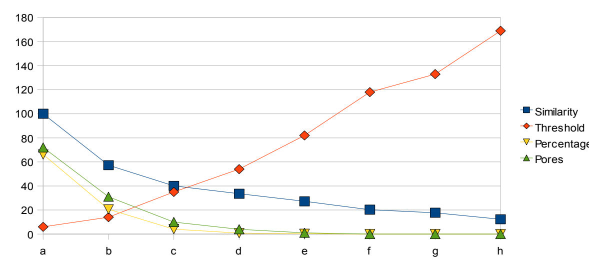


Figure 4: Anaysis of Test Case A

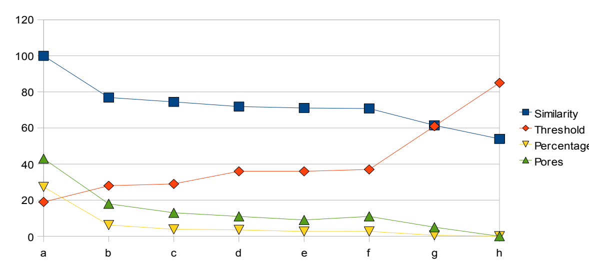


Figure 5: Anaysis of Test Case B

# 7 Analysis and discussion

The details of the ranking are compared in Figs. 4 and 5. The x axis of the diagrams directly corresponds to the sorted segments. Each line represents different characteristics of the images. The *Similarity* originates from the retrieval process and is scaled to a range between 0 (no similarity) and 100 (identity), according to Equ. 5. The values *Threshold* (Equ. 2 and *Percentage* (Equ. 1) represent the two components of the extracted *darkarea* feature. Finally, the *Pores* indicate the amount of retrieved pores in each image.

Three of the values are almost monotonically decreasing and show a certain correlation. Compared to the query image, the similarity to the other images is decreasing. At the same time, the percentage and the amount of detected pores is decreasing. The only ascending value is the *Threshold*, indicating the higher brightness of the subsequent images. In general, the gradients in Fig. 4 are higher than in Fig. 5. A slight inconsistency in the trends can be spotted between the amount of pores from images e and f in set B, where the value increases from 9 to 11, before dropping further down.

The trends of the diagrams support the previously perceived impression. While set A bears a high variation, set B is very homogeneous in the central part. The results are sorted according to their *similarity*. Both *threshold* and *percentage* are coupled to the *similarity*, as it is derived from those numbers. In fact, the most interesting correlation can be found between *similarity* and the amount of detected pores. Except from the small inconsistency in test case B, the images are basically sorted by amount of pores. This sorting has actually been achieved by a very simple feature vector without any deeper knowledge about the semantics.

Judging the samples manually shows that the actual amount of gas pores is often higher than the extracted one. This is caused due to the fact that the circle extraction algorithm does not adjust itself to the varying conditions. While many sample images contain very dark areas, in some images the defects are merely a grey shade instead of a clear black area. Additionally, the x-ray images show a two dimensional projection of a three dimensional object. This easily causes overlaps of distinct pores, blurring the borders between them.

# 8 Conclusion

## 8.1 Achievements

It is shown that CBIR techniques can be applied to the engineering domain, in this case welding. In sufficiently controlled environments, the suggested feature extraction algorithms could be applied. A highly specialized solution is not always required. The use of an existing CBIR search engine for the analysis permitted a very short implemetation time for the suggested features. Further, the system automatically provides a solution for archiving and organizing the digitized images. The software could be a useful tool for training in the weld profession and related areas in engineering.

## 8.2 Future research

The direct search for circular defects is one use case that will be investigated more deeply in the future. Especially a parallel pre-processing step to extract edges is expected to be advantageous in handling intersecting areas and stronger variations in the background colours. A second class of defects to be examined is the crack, which can also be revealed with edge detection algorithms. For those, the length and direction can be extracted.

# 9 Acknowledgements

This project has been funded with support from the European Commission. This publication reflects the views only of the author, and the Commission cannot be held responsible for any use which may be made of the information contained therein.

*References:*

[1] Marion Borowski, Lars Brocker, Stephan Heisterkamp, and Jobst Loffler. Structuring the Visual Content of Digital Libraries Using CBIR Systems. *IV '00: Proceedings of the International Conference on Information Visualisation*, 00:288, 2000.

[2] R Boyle and R Thomas. *Computer Vision: A First Course*. Blackwell Scientific Publications, 1988.

[3] Benjamin Bustos, Daniel Keim, Dietmar Saupe, Tobias Schreck, and Dejan Vranić. An experimental effectiveness comparison of methods for 3D similarity search. *International Journal on Digital Libraries*, 6(1):39–54, 2005.

[4] Ding-Yun Chen, Xiao-Pei Tian, Yu-Te Shen, and Ming Ouhyoung. On Visual Similarity Based 3D Model Retrieval. In *Eurographics*, pages 223–232, Granada, Spain, 2003.

[5] Ritendra Datta, Weina Ge, Jia Li, and James Z. Wang. Toward bridging the annotation-retrieval gap in image search by a generative modeling approach. In *MULTIMEDIA '06: Proceedings of the 14th annual ACM international conference on Multimedia*, pages 977–986, New York, NY, USA, 2006. ACM.

[6] J.P. Eakins and M.E. Graham. Content-based Image Retrieval. A Report to the JISC Technology Applications Programme. Technical report, University of Northumbria at Newcastle, January 1999.

[7] Anuj R. Jaiswal, C. Lee Giles, Prasenjit Mitra, and James Z. Wang. An architecture for creating collaborative semantically capable scientific data sharing infrastructures. In *WIDM '06: Proceedings of the 8th annual ACM international workshop on Web information and data management*, pages 75–82, New York, NY, USA, 2006. ACM.

[8] Hai Jin, Aobing Sun, Ran Zheng, Ruhan He, Qin Zhang, Yingjie Shi, and Wen Yang. Content and semantic context based image retrieval for medical image grid. In *GRID*, pages 105–112. IEEE, 2007.

[9] Ying Liu, Dengsheng Zhang, Guojun Lu, and Wei-Ying Ma. A survey of content-based image retrieval with high-level semantics. *Pattern Recognition*, 40:262–282, 2007.

[10] Andrzej Materka and Piotr Cichy. Texture analysis of x-ray image for detection of changes in bone mass and structure. Technical report, Institute of Electronics, Technical University of Łódź.

[11] Henning Müller, Paul Clough, William Hersh, Thomas Deselaers, Thomas Lehmann, and Antoine Geissbuhler. Evaluation axes for medical image retrieval systems: the imageCLEF experience. In *MULTIMEDIA '05: Proceedings of the 13th annual ACM international conference on Multimedia*, pages 1014–1022, New York, NY, USA, 2005. ACM.

[12] Raoul Pascal Pein, Milton Amador, Joan Lu, and Wolfgang Renz. Using CBIR and Semantics in 3D-Model Retrieval. In *Computer and Information Technology, 2008. CIT 2008. 8th IEEE International Conference on*, pages 173–178, July 2008.

[13] Raoul Pascal Pein, Joan Lu, and Wolfgang Renz. An Extensible Query Language for Content Based Image Retrieval based on Lucene. In *Computer and Information Technology, 2008. CIT 2008. 8th IEEE International Conference on*, pages 179–184, July 2008.

[14] Raoul Pascal Pein and Zhongyu Lu. Content Based Image Retrieval by Combining Features and Query-By-Sketch. In Hamid R. Arabnia and Ray R. Hashemi, editors, *IKE*, pages 49–55. CSREA Press, june 2006.

[15] Raoul Pascal Pein and Zhongyu Lu. A Flexible Image Retrieval Framework. In Yong Shi, G. Dick van Albada, Jack Dongarra, and Peter M. A. Sloot, editors, *International Conference on Computational Science (3)*, volume 4489 of *Lecture Notes in Computer Science*, pages 754–761. Springer, may 2007.

[16] Ben Shneiderman, Benjamin B. Bederson, and Steven M. Drucker. Find that photo!: interface strategies to annotate, browse, and share. *Commun. ACM*, 49(4):69–71, 2006.